IEEE Access
Multidisciplinary | Rapid Review | Open Access Journal

SPECIAL SECTION ON IEEE POWER & ENERGY SOCIETY SECTION

Received 27 May 2025, accepted 8 June 2025, date of publication 12 June 2025, date of current version 24 June 2025.

Digital Object Identifier 10.1109/ACCESS.2025.3579320

RESEARCH ARTICLE

Effect of Bulk Capacitor on Harmonics of Energy-Efficient Devices

KAMRAN DANIEL[1,2], (Member, IEEE), LAURI KÜTT[1], (Senior Member, IEEE), NOMAN SHABBIR[3,4], (Senior Member, IEEE), MUHAMMAD NAVEED IQBAL[1,5], JOÃO F. MARTINS[4], (Senior Member, IEEE), MATTI LEHTONEN[2], (Member, IEEE), AND PÄIVO SIMSON[6]

[1]Department of Electrical Power Engineering and Mechatronics, Tallinn University of Technology, 19086 Tallinn, Estonia
[2]Department of Electrical Engineering and Automation, Aalto University, 02150 Espoo, Finland
[3]FinEst Centre for Smart Cities, Tallinn University of Technology, 19086 Tallinn, Estonia
[4]NOVA School of Science and Technology, CTS-UNINOVA, LASI, NOVA University Lisbon, 2829-516 Caparica, Portugal
[5]Staffordshire Centre for Renewable and Sustainable Engineering, University of Staffordshire, ST4 2DE Stoke-on-Trent, U.K.
[6]Department of Cybernetics, Tallinn University of Technology, 19086 Tallinn, Estonia

Corresponding author: Noman Shabbir (noman.shabbir@taltech.ee)

This work was supported in part by Estonian Research Council via Projects PRG2055, and in part by the Project "Increasing the Knowledge Intensity of Ida-Viru Entrepreneurship" co-funded by European Union under Grant 2021-2027.6.01.23-0034.

ABSTRACT This paper develops analytical expressions to describe the behavior of harmonic components in rectifier circuits. It examines how harmonic content in the supply voltage influences the harmonic currents drawn by energy-efficient loads. By analyzing these interactions, the study provides insights into circuits integrating single-phase AC/DC converters, such as LED lamps. The findings emphasize the interdependence between harmonic phase angles and their impact on load current harmonics, which is essential for understanding supply voltage distortions and their effects on electrical loads. The assumptions established in this study support the development of more accurate models for characterizing load harmonic currents, enhancing the predictive capabilities of harmonic estimation methods. Furthermore, the proposed computational approach determines key rectifier performance parameters, including peak voltage across the bulk capacitor and the peak time relationship with harmonic components of the voltage waveform. These insights provide a deeper understanding of rectifier circuit behavior under distorted supply conditions, demonstrating the quantifiable impact of harmonic phase angles on rectifier capacitor dynamics offering practical implications for harmonic analysis, and performance optimization. The analytical framework developed here enables a more precise characterization of peak voltage timing and magnitude, which is critical for evaluating rectifier operation under various harmonic conditions.

INDEX TERMS Harmonic modeling, rectifier circuits, ac/dc converters.

I. INTRODUCTION

In electrical supply systems, the presence of harmonics can lead to an elevation in peak voltage levels [1]. In order to comprehensively grasp this issue, it is essential to first investigate the impact of harmonics on voltage waveforms. [2], [3], [4]. Harmonics are typically produced by nonlinear loads, including devices like switch mode power supplies, variable speed drives, and other electronics that draw non-sinusoidal current from the power source [5], [6], [7], [8], [9]. These loads cause a distortion in the current waveforms they draw, resulting in an alteration of peak voltage characteristics [10], [11]. This distortion manifests when the voltage waveform peaks exceed those of an ideal sinusoidal waveform, resulting from harmonic currents generated by nonlinear loads [12], [13], [14]. The supply voltage waveform can be described as:

$$u_{LVAC}(t) = u_1(t) + u_2(t) + u_3(t) + \ldots + u_n(t) \quad (1)$$

The associate editor coordinating the review of this manuscript and approving it for publication was K. Srinivas.

$$u_{LVAC}(t) = U_{1M}\cdot sin\,(\omega_1 t + \varphi_1) + U_{2M}\cdot sin\,(\omega_2 t + \varphi_2) + \ldots + U_{NM}\cdot sin\,(\omega_N t + \varphi_N) \quad (2)$$

Here $u_1(t)$ is the fundamental voltage component having magnitude U_{1M}, frequency ω_1 and phase angle φ_1, also U_{NM}, ω_N and φ_N, are magnitude, frequency and phase angle of the nth voltage harmonic in supply u_{LVAC}(t).

Ideally, the series expression in equation (1) includes all harmonics, but in practice, the odd-order harmonics dominate the waveform [15]. The dominance of odd harmonic content can be attributed to the repetitive characteristics of the waveform. Notably, even-order harmonics gain significance primarily in the presence of variations in waveform shape that occur from one cycle to the next [16]. Accordingly, in this study, only odd-order harmonics will be taken into consideration, while even-order harmonics are presumed to possess a magnitude of zero.

The peak time (t_{Peak}) of a voltage waveform depends on the amplitude and phase angle of the voltage harmonics [1], [16], [17], [18]. This t_{Peak} corresponds to the end-of-conduction moment of the rectifier's current [19], [20]. Consequently, the harmonics present in the load current are also influenced by the resulting delay in the peak voltage. References [8] and [21] provides a performance comparison of different models under non-sinusoidal supply conditions.

In an ideal sinusoidal signal, the expected peak typically occurs at an angle of 90 degrees. However, the presence of voltage harmonics within the supply can lead to an alteration of this peak, causing it to deviate from its anticipated position at 90 degrees [22]. The type and amount of load connected to the network changes continuously, which impacts the voltage at the point of common connection (PCC). As a result, the supply voltage may contain multiple harmonics with varying magnitudes and phase angles [23]. FIGURE 1 illustrates the resultant flat and pointed top waveforms commonly observed as supply voltage in low-voltage (LV) networks. In both cases, the available top voltage for charging the rectifier's capacitor will vary, causing differences in the progression and the end of the conduction cycle [24].

Existing studies on rectifier circuits predominantly emphasize harmonic magnitudes, often neglecting the significant influence of harmonic phase angles on peak voltage timing and load current behavior. Most models are based on ideal sinusoidal conditions or rely on computational simulations, which inherently constrain their accuracy concerning real-world applications, such as LED drivers. These limitations hinder the reliable prediction of rectifier performance under distorted supply voltages, which is critical for the design of energy-efficient devices. This study confronts these challenges by proposing a phase-angle-dependent analytical framework for rectifier circuits. In contrast to prior research that has mainly concentrated on harmonic magnitudes, the proposed methodology will assess the combined effects of harmonic magnitudes and phase angles on peak voltage timing and capacitor charging dynamics. Analytical expressions for essential parameters will be systematically derived, providing a more precise characterization of rectifier behavior under voltage distortion. Additionally, this research will integrate experimental validation to validate theoretical findings, illustrating how specific harmonic phase shifts can significantly influence rectifier operational characteristics.

A brief comparison with estimation models and techniques from the literature is provided in table 1.

TABLE 1. Brief comparison of harmonic estimation techniques.

Model/ Technique	Harmonic Magnitude	Harmonic Phase Angle	Load/ Network Interaction	Experimental Validation	Limitation
Constant Current Model [3] , [25]	yes	no	no	partial	Ignores phase-angle effects
Norton Model [26]	yes	partial	partial	partial	Limited load/network coupling
Frequency-Coupled Martix Model [27], [28]	yes	yes	partial	yes	Linear assumption, phase effect often ignored
Stochastic Models [29]–[31]	yes	no	no	no	Aggregate, not device-specific
Proposed Method	yes	yes	yes	yes	Single-phase, idealized load focus

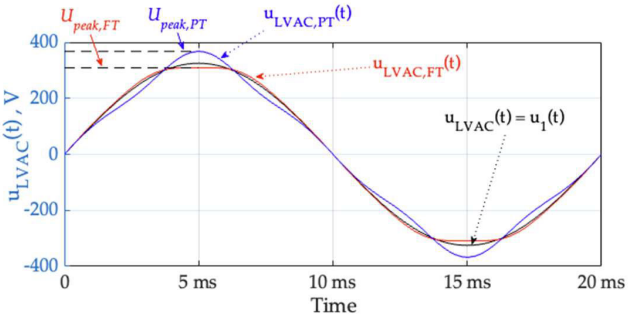

FIGURE 1. Voltage pure-sine flat-top(FT) & pointed-top(PT) waveforms (maximum charge on capacitor for flat and pointed top waveforms).

The novelties of this work are as follows:

1. This study presents a phase-angle-dependent methodology for the analysis of rectifier circuits, redirecting attention from mere harmonic magnitudes to the interactive impact of both magnitude and phase shifts. Through a thorough evaluation of how voltage harmonics affect the timing of conduction, this research significantly improves the modeling of rectifier behavior in response to distorted supply conditions.
2. A novel analytical framework has been developed to ascertain peak voltage timing in rectifier circuits functioning under non-ideal supply voltages, accommodating nonlinear harmonic interactions that play a critical role in capacitor charging and the timing of conduction cut-off points.
3. Furthermore, this investigation incorporates comprehensive experimental validation to assess harmonic sensitivity in energy-efficient loads. The results indicate that certain

harmonic phase angles exert an influence on rectifier functionality, resulting in notable alterations in peak voltage and the duration of conduction.

The paper is structured as follows: Section II outlines the role of the capacitor in rectifier operation. Section III details the algorithm used to generate various waveforms and describes the measurement setup. Section IV presents the analytical expressions for key characteristic points of the supply waveform, which are critical for load current harmonics. Finally, Section V discusses and verifies the results.

II. RECTIFIER OPERATION

To optimize energy conversion using the natural conduction properties of diodes, a full-wave rectifier is the preferred option [32]. This rectifier is commonly built using a bridge connection of four diodes. FIGURE 2 and FIGURE 3 illustrate a typical bridge rectifier setup along with its input and output voltage waveforms. The output maintains a consistent DC current polarity throughout the AC cycle. For each half-cycle, two diodes are responsible for conducting the current [33].

However, during portions of the AC cycle with low instantaneous voltage, challenges arise. These sections result in reduced DC output power [34]. To ensure a steady DC power supply to the load during these intervals, it is common practice to include an energy storage element [35]. A bulk storage capacitor, denoted as C_B, is often placed in parallel with the load for this purpose, as shown in FIGURE 2.

FIGURE 4 and FIGURE 5 illustrate the general trends and equations governing the capacitor's charging and discharging processes [36]. When the rectifier's output voltage decreases after reaching its peak (at T/4 or 3T/4, where T is the time period of the input waveform, with T = 20 ms for a 50 Hz AC supply), the capacitor's voltage $u_{CB}(t)$ momentarily exceeds the instantaneous AC supply voltage $u_{LVAC}(t)$.'

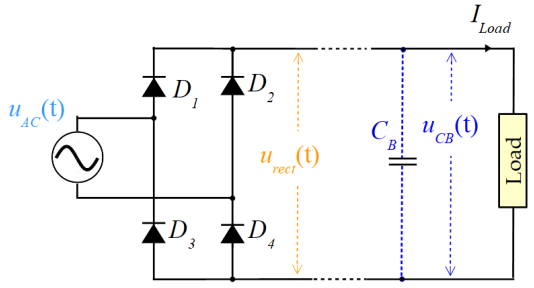

FIGURE 2. Ideal bridge (full wave) rectifier with capacitor.

At this point, all diodes stop conducting, and the capacitor begins supplying current to the load. This marks the start of a voltage drop in $u_{CB}(t)$. Once the absolute instantaneous value of the AC supply voltage surpasses the capacitor voltage, diodes D_2 and D_3 conduct during the negative half-cycle, recharging the capacitor. The capacitor's voltage then follows the AC voltage and reaches the peak output level U_{peak}

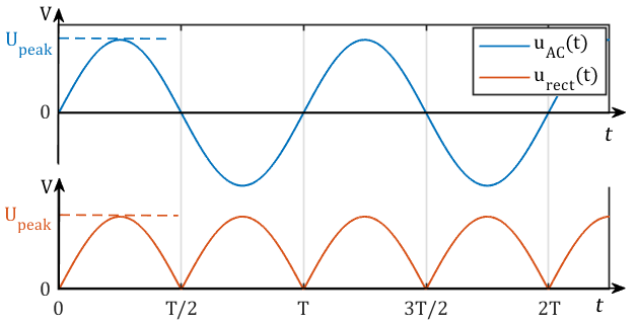

FIGURE 3. Input and output of full wave rectifier circuit.

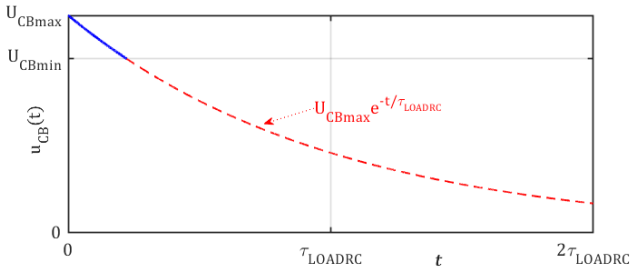

FIGURE 4. Capacitor discharging trend. Figure 2.10.

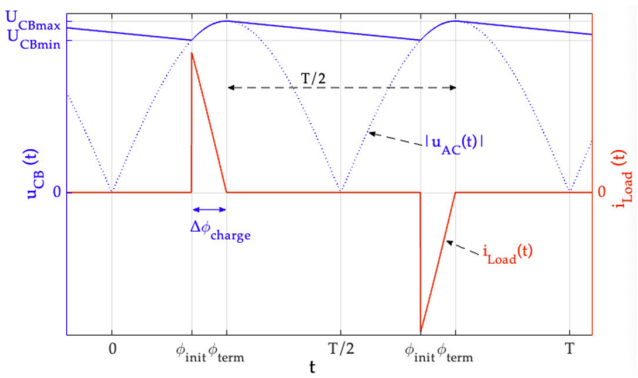

FIGURE 5. Characteristic waveforms for capacitor-equipped full-bridge rectifier.

again [37]. This process is depicted graphically in FIGURE 3 and FIGURE 5.

The conduction period of the diodes occurs between the initiation (ϕ_{init}) and termination (ϕ_{term}) phases of the capacitor's charging. The duration of this charging phase is defined as:

$$\Delta\varphi_{charge} = \varphi_{term} - \varphi_{init} \tag{3}$$

The capacitor's voltage variation, or ripple (ΔU_{ripple}), is expressed as

$$\Delta U_{ripple} = U_{CBmax} - U_{CBmin} \tag{4}$$

For a full-bridge rectifier circuit, the capacitor voltage peaks every T/2. After the termination of conduction at ϕ_{term}, the voltage decay is determined by the time $\tau_{LOADRC} = R_{DCL}\cdot$

C_B, where R_{DCL} is the resistance of the load connected to the capacitor (DC output) [38]. The charging behavior of the capacitor C_B is defined by (5).

$$u_{CB}(t) = U_{CBinit} + (U_{CBmax} - U_{CBinit})\left(1 - e^{-\frac{t-t_{term}}{\tau_{LOADRC}}}\right) \tag{5}$$

Here, t represents the time value greater than the termination of conduction (t_{term}) but less than the initiation of conduction in the next cycle (t_{init}). For the condition where $\tau_{LOADRC} \gg \{T/2 - \Delta\varphi_{charge}($ or $\Delta t_{charge})\}$, the capacitor's discharging can be approximated as a straight line, where its voltage decreases from U_{CBmax} to U_{CBmin} [39]. This is shown as the blue line in FIGURE 4. All in all, in full-wave bridge rectifier circuits, the ripple and capacitor's charging behaviour is determined by load resistance and capacitor value, as shown in equations (3)-(5) and FIGURE 5.

III. SUPPLY VOLTAGE WAVEFORM CONTROL AND CURRENT OUTPUT RESPONSE

To simulate various distorted supply voltage scenarios, a test platform was designed to generate supply voltage waveforms based on a specified table of parameters. The voltage control system was aimed at achieving precise adjustment of voltage harmonics, including their amplitude and injection phase angle.

To simulate various distorted supply voltage scenarios, a test platform was developed to generate voltage waveforms based on predefined parameter tables. The voltage control system precisely adjusts harmonic components, including their amplitude and injection phase angle.

Accurate measurement of current harmonic sensitivity requires accounting for small proportional variations. To ensure reliable sensitivity analysis, voltage supply conditions must remain highly stable. Thus, the regulation system must maintain a consistent output voltage regardless of fluctuations in the laboratory supply network or load variations. One method to achieve this stability is software-generated waveforms, where discrete momentary values are computed and transmitted to a digital-to-analog (DA) converter. A harmonic sensitivity identification system, designed to ensure voltage stability.

For comprehensive frequency response characterization, the measurement and waveform generation systems establish a platform for harmonic sensitivity evaluation. The phasor approach is used to analyze harmonic current sensitivity, with voltage waveforms defined by adjustable magnitude and phase angle.

A scanning procedure introduces a voltage harmonic component with a fixed magnitude into the supply voltage while varying its phase angle incrementally across 360 degrees. For each generated voltage condition, the load current I_{load} is measured.

A. MEASUREMENT SETUP

A test bench has been designed to facilitate the measurement of load devices, with the capability to support up to 16 loads simultaneously. The outputs from these loads are connected to a central distribution bus-bar, which is managed via relays for controlled operation. A general-purpose data acquisition system (DAQ) is employed to provide an analog reference signal for controlling the power supply.

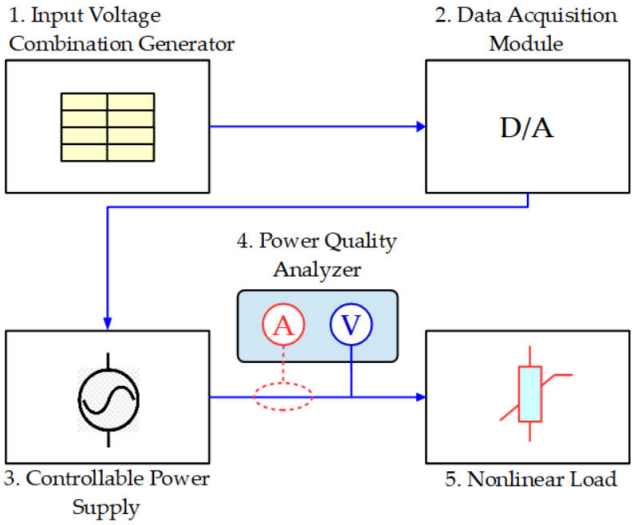

FIGURE 6. Test/measurement setup [41].

To achieve the required voltage waveform, a programmable power supply, Omicron-C356, is utilized. The power supply operates under the control of the reference signal, which is generated and transmitted by the DAQ system. This configuration enables precise control and monitoring of the voltage supply for the test bench.

The magnitude and phase angles of each odd harmonic are used to generate the reference signal for the programmable power supply. The equation provided below calculates $u_{test}(t)$ based on the amplitude and phase angles of the fundamental frequency and odd harmonics up to the 19th harmonic.

$$u_{test}(t) = \sum_{y=1}^{n} \sqrt{2} U_h \sin(2\pi f_h t + \varphi_{Uh}) \tag{6}$$

U_h represents the RMS value of a specific harmonic, while ϕ_{Uh} denotes the phase angle of that harmonic. The harmonic frequency is indicated by f_h. The measurement setup is designed to comply with the guidelines outlined in the IEC 61000-4-30 standard [40]. FIGURE 6 illustrates the block diagram of the measurement setup.

During the load characteristic scan, small but consistent and repeatable variations in the phase and magnitude of the harmonic current components were observed. These variations were verified by applying a discrete Fourier transform (DFT) to the current waveform recorded by the measurement instrument.

B. MEASUREMENT OUTCOME AND INITIAL OBSERVATIONS

The selection of LEDs was tested to establish the harmonic sensitivity fine-scale dataset. The focus was on the circuit type A lamps. In essence, the current waveforms of all the tested LEDs indicated similar type variation response characteristics to voltage harmonics added to the input voltage.

Time-domain observation of the scan outcome is presented FIGURE 7 as it compares the current waveform of an LED lamp when powered by a pure sinewave supply against when the supply voltage has an additional distinct harmonic voltage component at a specific magnitude and phased relative to the fundamental harmonic. It illustrates a scan result of the current waveforms outcome, when the 5th voltage harmonic was introduced in supply with a fixed magnitude level, and the harmonic injection phase angle changed in 15-degree steps. The synchronization of measured current waveforms was with respect to the zero-phase instant of the voltage waveform's fundamental harmonic.

A distinguishing parameter of the load current waveform is the instant of rectifier conduction initiation time instant t_{init}. At this time instant or very near to it, the load current provides the highest slope and achieves its peak value soon after this. Such rectifiers' current instantaneous peaks provide a characteristic quantity for the rectifier's current magnitude.

To put this all together, the deveoped test plateform with programable power supply and DAQ generates supply voltage waveform with controlled harmonic amplitudes for load testing, defined by (6). LED current waveforms show variation in peak value and conduction time with added voltage harmonic in supply.

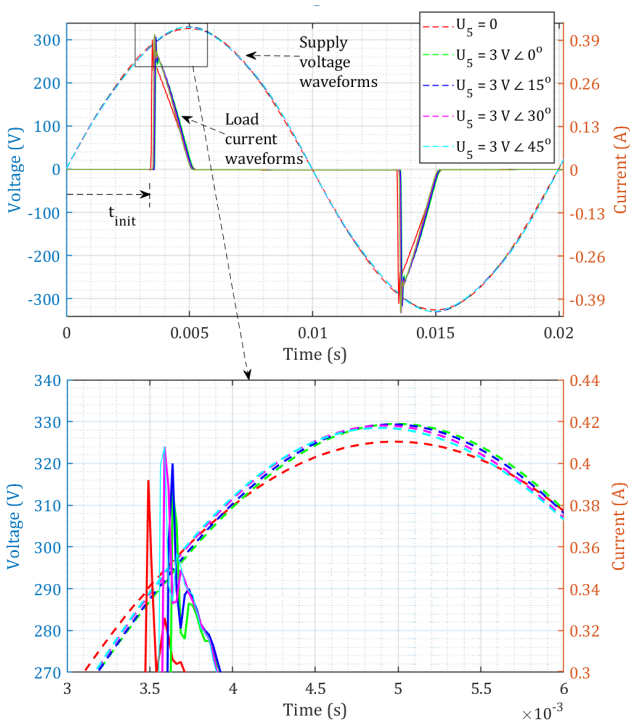

FIGURE 7. Current waveform initiation time and peak values affected by the 5th-order voltage harmonic phase angle in supply. Supply waveforms (dashed lines) and load current waveforms (continuous lines).

IV. TRIANGLE EXPRESSIONS OF TIME DOMAIN RESPONSE OF RECTIFIER CIRCUIT IN COMMON LOAD

This section presents an analytical approach to deriving a generalized expression for rectifier circuit operation. The derivation establishes a framework for determining the peak voltage timing (linked to rectifier diode conduction cut-off) and peak voltage level (corresponding to bulk capacitor voltage at conduction cut-off). This analysis forms the basis for modeling AC load current harmonics in rectifier-based devices under distorted supply conditions.

Most energy-efficient devices available in the market include rectifier circuits. FIGURE 8 illustrates the rectifier circuit commonly found in energy-efficient LED lamps. The operation of rectification depends on the shape of the supply voltage waveform. When the rectified voltage across the capacitor terminals reaches its peak value, the current conduction stops [42], [43], [44], [45]. The time at which conduction ends varies according to the peak voltage instant of the supply voltage waveform [46], [47]. The influence of different supply voltage harmonics on rectifier circuit operation has been empirically analyzed in [11], [13], and [48]. This study focuses on an A-type waveform, representative of low-cost LED lamps.

Triangular waveforms are widely used in signal processing due to their simple harmonic structure. Constructed by summing odd harmonics of a sine wave, their harmonic amplitudes decrease proportionally to the square of the harmonic number. This predictable pattern aids in various analytical applications. The linear rise and fall of triangular waves make them effective approximations for signals with sharp transitions, facilitating nonlinear system analysis.

To derive an analytical expression, it is crucial to recognize that harmonic components originate from the time-domain representation of the waveform. Variations in load current harmonics result from changes in the time-domain current waveform. Thus, the analytical formulation of harmonic components is based on time-domain current behavior, particularly for LED lamp AC loads, which operate through rectifiers.

The rectification process is influenced by the supply voltage waveform, as demonstrated through circuit analysis and experimental observations. An LED lamp typically includes a rectifier, a bulk capacitor C_B (FIGURE 8), and a driver circuit. While previous studies have extensively analyzed rectifier behavior, this discussion assumes an idealized circuit model to focus on the analytical structure of harmonic currents. A more detailed circuit model would offer minimal improvements in accuracy at this stage. Comprehensive circuit analysis will be addressed in future research.

To simplify the analytical observations, certain assumptions are made, and the current waveform is analyzed using a basic framework:

1. The LED load current waveform is assumed to have a triangular shape. The slope of the load current is considered a linear function that changes with time (as shown by the dotted black line in FIGURE 9).
2. The time points t_{init} and $t_{i,peak}$ are assumed to be nearly identical, effectively occurring at the same moment, t_{init}.
3. The three vertices of the triangular waveform are used to define the load current function (dotted black line). This function is derived by calculating the slope between two points,, ($\{t_{init},\ i_{L,peak}\}$ and $\{t_{peak},\ 0\}$), using the slope formula based on these points.

$$\frac{t - t_{init}}{t_{peak} - t_{init}} = \frac{i_{Load}(t) - I_{Load,peak}}{0 - I_{Laod,peak}} \tag{7}$$

$$i_{Load}(t) = \frac{-(t - t_{init})\, I_{Laod,peak}}{t_{peak} - t_{init}} + I_{Load,peak} \tag{8}$$

   where $i_{L,peak}$ represents the peak value of load current.
4. The time points t_{term} and t_{peak} are assumed to be very close, effectively occurring at the same moment, t_{peak}.
5. It is assumed that U_{CBmax} is reached when U_{LVAC} hits its peak value. The conduction of the rectifier is considered to stop immediately after this peak.

The specifications of the resulting triangular waveform are shown in FIGURE 10.

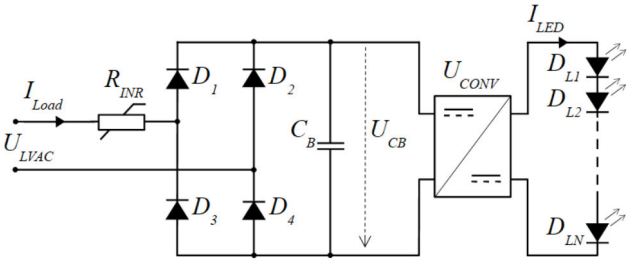

FIGURE 8. Rectifier circuit in LED lamp [49].

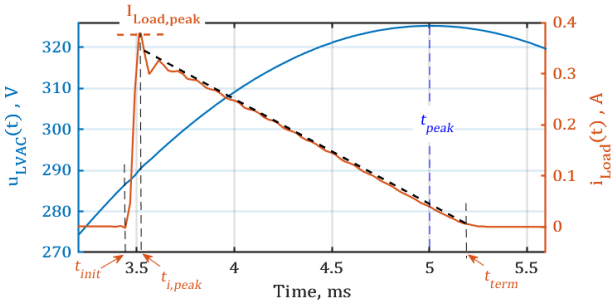

FIGURE 9. Close-up of conduction half-cycle of a rectifier current.

Empirical results from Section III indicate that the t_{init} and I_{peak} values directly influence the harmonic characteristics. Therefore, the model waveform shown in FIGURE 10 is based on these same variables. The current waveform, $i_{Load}(t)$, does not exhibit odd or even symmetry but follows

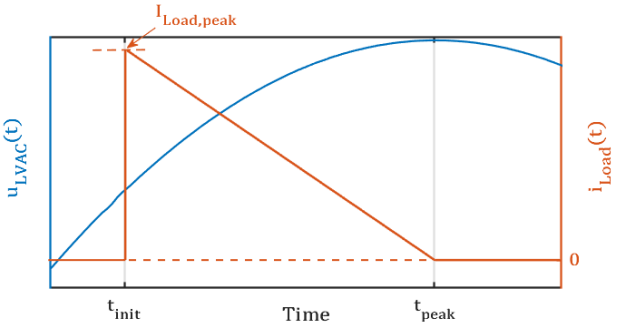

FIGURE 10. Triangular shape assumption of the load current, characteristic points/limits for Fourier equations.

half-wave symmetry. This aligns with the half-wave symmetry principle of the Fourier series.

$$f\left(t - \frac{T}{2}\right) = -f(t) \tag{9}$$

And the Fourier coefficients for *half-wave* symmetry become

$$a_0 = 0$$

$$a_n = \begin{cases} \dfrac{4}{T}\displaystyle\int_0^{T/2} f(t)\cos(nt)dt & \textit{for n odd} \\ 0 & \textit{for n even} \end{cases}$$

$$b_n = \begin{cases} \dfrac{4}{T}\displaystyle\int_0^{T/2} f(t)\sin(nt)dt & \textit{for n odd} \\ 0 & \textit{for n even} \end{cases}$$

Using Equations (7) and (8), the Fourier coefficients for the load current (a_{niL} and b_{niL}) can now be determined

$$a_{n_I} = \frac{4}{T}\int_0^{T/2} i_{Load}(t)\, cos(n\omega_1 t)dt \tag{10}$$

Since the current is present only between t_{init} and t_{peak}, the limits of the definite integral are set accordingly

$$a_{n_{i_L}} = \frac{4}{T}\int_{t_{init}}^{t_{peak}} i_{Load}(t)\, cos(n\omega_1 t)dt \tag{11}$$

After solving the integral and placing the limits in *(11)*
Similarly solving b_n

The Fourier series of the current waveform can be determined using (12) or (14), as shown at the bottom of the next page, once the values of t_{init}, t_{peak}, and $I_{Load,peak}$ are known.

The derivation of the variables in (12) and (14) can proceed as follows:

1. t_{peak}, which corresponds to the instant when $U_{LVAC,max} = U_{peak}$, will be defined. This is the most definitive point of the supply waveform.
2. U_{peak} will be calculated using the value of t_{peak}.
3. U_{init}, the value at which current conduction begins, will be determined.
4. Using U_{init}, the corresponding value of *tinit* will be found.

5. With t_{init} known, the value of $I_{Load,peak}$ will be determined.

In the scope of this article, only the first two expressions, t_{peak} and U_{peak}, will be examined. FIGURE 11 presents the scope of this article.

To summarise this section, a mathematical approach is proposed to model the load current in rectifier circuit operation for LED lamps, focusing on peak voltage timing and current waveform shape (Figure 8-10, and equations (7)–(14)). The triangular load current model links t_{init}, t_{peak}, and $I_{Load,peak}$ to Fourier equations to define load current.

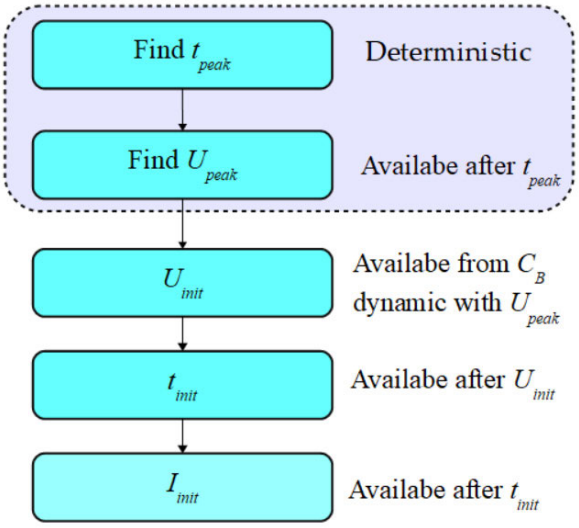

FIGURE 11. Scope of the paper for characteristic points.

V. ANALYTICAL EXPRESSION FOR PEAK VOLTAGE INSTANTS

A. VOLTAGE WAVEFORM NUMERICAL ANALYSIS

In discussing the impact of harmonics on peak voltage, it is important to account for how the phase angle of the harmonic voltage affects the supply waveform. One significant factor is the shift in the peak voltage moment ($\Delta\phi_{peak}$) caused by the harmonic voltage's phase shift, as shown in FIGURE 12. The resulting symmetrical patterns, depicted in FIGURE 13 and FIGURE 14, illustrate how a single voltage harmonic with varying amplitudes influences the shift in the peak voltage moment.

For the analysis, assume the supply voltage waveform in equation TABLE 2 includes two components: the main harmonic with a magnitude U_1 and a harmonic of order y with a magnitude U_y. The peak voltage at any instant can be calculated using the general sine wave expression as:

$$U_{Peak} = U_1 \cdot sin\left(\omega_1 \cdot t_{peak}\right) + U_y \cdot sin\left(y \cdot \omega_1 \cdot t_{peak} + \varphi_y\right) \tag{15}$$

or expressed in terms of the phase relative to the main harmonic (zero phase) as

$$U_{Peak} = U_1 \cdot sin\left(\varphi_{Peak}\right) + U_y \cdot sin\left(y \cdot \varphi_{Peak} + \varphi_y\right) \tag{16}$$

Here, the main harmonic starts at zero phase ($t = 0$), φ_y is the phase angle of the harmonic voltage component U_y relative to the main harmonic, and U_y represents the magnitude of the harmonic voltage component.

Analytically, the peak voltage instant (t_{peak}), corresponding to the end of the capacitor conduction, can be determined by finding where the derivative of the voltage approaches zero.

$$max\left\{u_{LVAC}(t)\right\} \Rightarrow \frac{du_{LVAC}(t)}{dt} = 0 \tag{17}$$

At this peak instant, the voltage across the capacitor (U_{CB}) in the rectifier circuit reaches its maximum value.

$$U_{CB_{MAX}} = max\left\{u_{LVAC}(t)\right\} / T_{50Hz} \tag{18}$$

Numerically, the peak voltage value can be calculated for any given U_y and ϕ_y using finite time-step calculations with (15).

A broader analytical approach is required to derive universally applicable expressions for peak voltage value and timing. Since harmonic voltage components can have any phase angle or magnitude, purely numerical descriptions may lack generality. The complexity of peak timing determination is evident in FIGURE 13 and FIGURE 14, which illustrate variations in peak phase range due to harmonics. These results reveal an eccentric periodic function, akin to those in Kepler's equations, which cannot be solved geometrically.

The peak voltage expressions are derived by analyzing the dynamics of the supply voltage's sinewave components. For

$$a_{n_{iL}} = \frac{4}{T}\left[\frac{i_{Load,peak}\left\{n\omega_1\left(t_{peak} - t_{init}\right) sin\left(n\omega_1 t_{iinit}\right) - cos\left(n\omega_1 t_{init}\right) + cos\left(n\omega_1 t_{peak}\right)\right\}}{n^2\omega_1^2\left(t_{init} - t_{peak}\right)}\right] \tag{12}$$

$$b_{n_{iL}} = \frac{4}{T}\int_{t_{init}}^{t_{peak}} i_{Load}(t)\, sin(n\omega_1 t)dt \tag{13}$$

$$b_{n_{iL}} = \frac{4}{T}\left[\frac{i_{Load,peak}\left\{n\omega_1\left(t_{init} - t_{peak}\right) cos\left(n\omega_1 t_{init}\right) - sin\left(n\omega_1 t_{init}\right) + sin\left(n\omega_1 t_{peak}\right)\right\}}{n^2\omega_1^2\left(t_{init} - t_{peak}\right)}\right] \tag{14}$$

the peak timing instant (t_{peak}), the first-order derivatives of the fundamental and harmonic components must be equal in magnitude:

$$\frac{d}{dt}u_1\left(t_{peak}\right) = -\frac{d}{dt}u_y\left(t_{peak}\right) \tag{19}$$

$$U_1{\cdot}\omega_1{\cdot}cos(\omega_1 t_{peak}) = -U_y{\cdot}\omega_1{\cdot}y{\cdot}cos(y\omega_1 t_{peak}+\varphi_y) \tag{20}$$

Simplified into

$$U_1{\cdot}cos(\omega_1 t_{peak}) = -U_y{\cdot}y{\cdot}cos(y\omega_1 t_{peak}+\varphi_y) \tag{21}$$

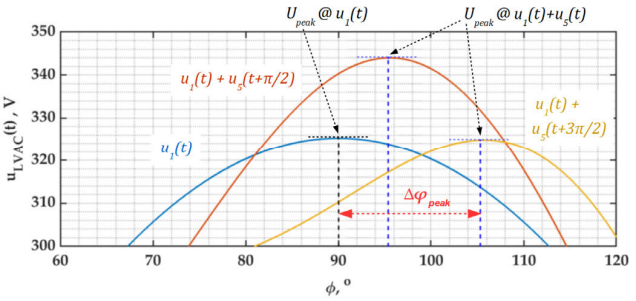

FIGURE 12. Peak instant response to harmonic phase angle.

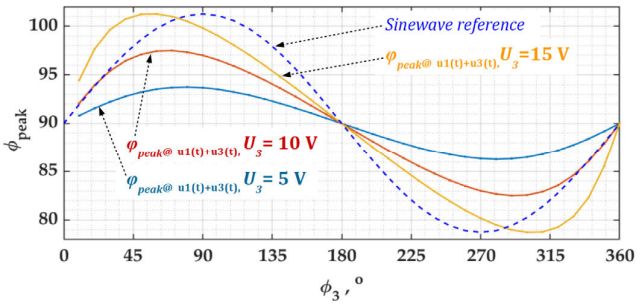

FIGURE 13. Variation in peak instant depending on harmonic phase angle.

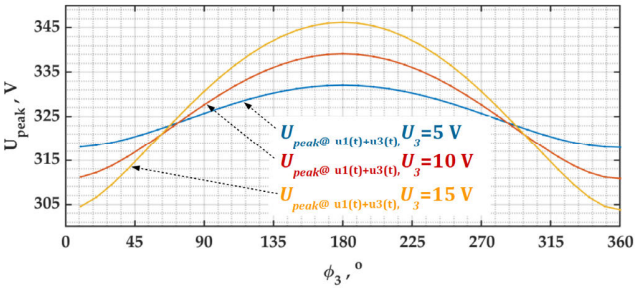

FIGURE 14. Variation in peak depending on harmonic phase angle.

Figures 12–14 demonstrate how the peak instant and value change with harmonic phase angle variations. Numerical results for ϕ_{peak} and U_{peak} reveal a periodic function that repeats every 360° phase rotation of ϕ_y. This periodicity allows the function to be expressed analytically as:

2) The function is basically a (co)sinusoidal form, where the argument is a function of U_y and φ_y.

$$U_{peak} = U_{1peak} + U_{peak,M}{\cdot}sin\left(\gamma_{Upeak}\right) \tag{22}$$

$$\varphi_{peak} = \varphi_{1peak} + \varphi_{peak,M}{\cdot}sin\left(\gamma_{\varphi peak}\right) \tag{23}$$

Here, $U_{Peak,M}$ represents the maximum difference between U_{1Peak} and the resultant peak voltage, and $\phi_{Peak,M}$ is the maximum difference between ϕ_{1Peak} and the resultant peak timing. γ_{UPeak} and $\gamma_{\phi Peak}$ are functions of the harmonic voltage level and phase angle.

Key points for these functions are described as

3) Case 1**:** At $U_{peak} = U_{1,peak} \pm U_{peak,M}$, the argument in equation (22) equals 90° or 270°.
4) Case 2**:** At $t_{peak} = t_{1,peak} \pm \Delta t_{peak,M}$, the argument in equation (23) equals 90° or 270°.
5) Case 3: At $U_{peak} = U_{1peak}$, the argument in equation (22) equals 0° or 180°.
6) In the final case, the peak timing points ($t_{peak} = t_{1,peak}$) coincide with the main harmonic's 90° or 270° phase instants (23).

B. DYNAMIC EXPRESSIONS FOR PEAK VOLTAGE INSTANT

With the addition of a single voltage harmonic, the dynamic variation of the peak voltage and its timing is shown in FIGURE 15. The characteristic cases for peak voltage observations are outlined below:

Case 1: Expressions for Maximum and Minimum Peak Voltage Magnitudes.

The maximum possible value of the peak voltage is observed when both $u_1(t_{peak})$ and $u_y(t_{peak})$ components reach their maximum values. In this case, the sum of their magnitudes determines U_{peak}. This happens when the sine components both yield a value of "1," corresponding to a sine argument of $\pi/2$:

$$U_{peak,max} = U_1{\cdot}\,sin\left(\frac{\pi}{2}\right) + U_y{\cdot}sin\left(\frac{\pi}{2}\right) \tag{24}$$

Given that the harmonic phase angle is y times higher than the main harmonic, the harmonic component's angle that aligns with $\pi/2$ at the peak of U_1 is:

$$\varphi_{y,peak,max} = y{\cdot}\,\pi/2 \tag{25}$$

For odd harmonics, a system with only a 3rd harmonic added will peak when $\phi_{U3} = -90\circ$, while a 5th harmonic will result in a maximum peak voltage when $\phi_{U5} = 90\circ$. Similarly, the minimum magnitudes occur when the harmonic phase angles are offset by 180∘.

Case 2: Maximum Shift in Peak Time from Fundamental Component Peak Time (90° or π/2)

The maximum time shift of the peak time instant, $t_{peak,\Delta\phi max}$, happens when the first derivative of the harmonic component is at its maximum. This can be expressed as**:**

$$\left\{\frac{d}{dt}u_y\left(t_{peak,\ \Delta\varphi_{max}}\right)\right\}_{max} = U_y{\cdot}y{\cdot}\omega_1 \tag{26}$$

Assuming equation (24), this occurs when $(y{\cdot}\omega{\cdot}t_{peak} + \phi_{Uy})$ equals zero. Thus, the peak phase shift for the harmonic occurs when

$$\varphi_{Uy} = y{\cdot}\,\omega_1{\cdot}t_{peak} \tag{27}$$

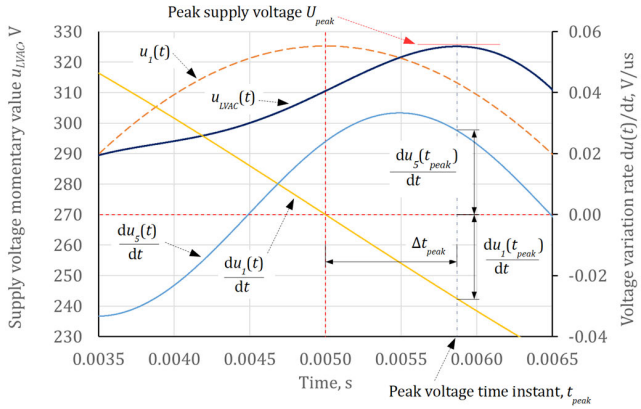

FIGURE 15. Variation in peak time instant depending on harmonic phase angle.

From (26)

$$cos\left(\omega_1 t_{peak,\ \Delta\varphi_{max}}\right) = \frac{U_y}{U_1} y \tag{28}$$

and replacing

$$A = \frac{U_1}{U_y} \tag{29}$$

The expression will be:

$$t_{peak,\ \Delta\varphi_{MAX}} = \frac{1}{\omega_1} cos^{-1}\left(\frac{y}{A}\right) \tag{30}$$

Case 3: Instant When Peak Voltage of Combined Waveform Equals Fundamental Harmonic Peak.

This case corresponds to the point where the peak voltage of the combined waveform ($U_1 + U_y$) equals the peak magnitude of the fundamental harmonic (U_1):

$$U_1 = U_1\, sin(\omega_1 \cdot t) + U_x\, sin(y\omega_1 t + \varphi_y) \tag{31}$$

Here, U_1 is the magnitude of the fundamental component, which for 230 V RMS is approximately 325 V. U_y represents the amplitude of the supply voltage harmonic component, and ϕ_y is the phase angle of the voltage harmonic.

The crossing point of the harmonic (U_y) near 90° of the fundamental harmonic can be calculated as:

$$t_{cross,y} = \frac{T_1}{y}\left(\frac{1}{4}(y+1) - \frac{\varphi_y}{2\pi}\right) \tag{32}$$

$$\varphi_{cross,y} = 2\pi \frac{t_{cross,y}}{T_1} \tag{33}$$

where y is the harmonic order and T_1 =0.02s is the time period of the fundamental harmonic. Transforming Equations (15) and (16) into the phase angle domain

$$U_1 = U_1\, sin\left(90° - \varphi_{peak}\right) + U_y\, sin\,\varphi_{y,c} \tag{34}$$

$$U_1\, cos\left(90° + \varphi_{peak}\right) = -y \cdot U_y \cdot cos\,\varphi_{y,c} \tag{35}$$

Here ϕ_{peak} is the phase distance between the peak of the fundamental component (i.e. 90° or $\pi/2$) and the peak of $u_{LVAC}(t)$ expressed in degrees on the fundamental harmonic scale and $\phi_{y,c}$ is the distance between the peak of $u_{LVAC}(t)$ and the zero crossing instant of the voltage harmonic component.

From (34)

$$sin\,\varphi_{y,c} = \frac{U_1}{U_y} - \frac{U_1}{U_y} sin\left(90° - \varphi_{peak}\right) \tag{36}$$

$$sin\,\varphi_{y,c} = A\,[1 - cos\,\varphi_{peak}] \tag{37}$$

From (35)

$$\frac{U_1}{U_y \cdot y} cos\left(90° + \varphi_{peak}\right) = -cos\,\varphi_{y,c} \tag{38}$$

As *cos* is an even function

$$\frac{A}{y} cos\left(90° + \varphi_{peak}\right) = cos\,\varphi_{y,c} \tag{39}$$

$$\frac{A}{y} cos\left(90° + \varphi_{peak}\right) = 1 - [sin\,\varphi_{y,c}]^2 \tag{40}$$

$$sin\,\varphi_{y,c} = \sqrt{1 - \left[\frac{A}{y} cos\left(90° + \varphi_{peak}\right)\right]^2} \tag{41}$$

Equating (37) and (41) provides

$$A^2[1 - cos\left(\varphi_{peak}\right)]^2 = 1 - \left[\frac{A}{y} cos\left(90° + \varphi_{peak}\right)\right]^2 \tag{42}$$

and this can be developed into

$$\left[A^2 - \frac{A^2}{x^2}\right](cos\,\varphi_{peak})^2 - 2A^2\, cos\,\varphi_{peak} + \cancel{+A^2} + \frac{A^2}{y^2} - 1 = 0 \tag{43}$$

Substituting Q= cos(ϕ_{peak})

$$\left[1 - \frac{1}{y^2}\right] \cdot Q^2 - 2 \cdot Q + 1 + \frac{1}{y^2} - \frac{1}{A^2} = 0 \tag{44}$$

Coefficients of quadratic equations are

$$a = \left(1 - \frac{1}{y^2}\right),\ b = -2 \text{ and } c = 1 + \frac{1}{y^2} - \frac{1}{A^2}$$

where Q=cos(ϕ_{peak}). Solving this quadratic equation yields the values for ϕ_{peak}, while similar expressions for $\phi_{y,c}$ can be derived using equations (34) and (35).

$$sin\left(90° - \varphi_{peak}\right) = 1 + \frac{U_y}{U_1} sin\,\varphi_{y,c} \tag{45}$$

And

$$cos\,\varphi_{peak} = 1 + \frac{sin\,\varphi_{y,c}}{A} \tag{46}$$

Now (35) becomes

$$cos\left(90° + \varphi_{peak}\right) = -\frac{U_y}{U_1} \cdot y \cdot cos\,\varphi_{y,c} \tag{47}$$

$$-sin\,\varphi_{peak} = -\frac{y \cdot cos\,\varphi_{y,c}}{A} \tag{48}$$

Squaring and adding (46) and (48)

$$\left(\frac{y\cdot cos\,\varphi_{y,c}}{A}\right)^2+\left(1+\frac{sin\,\varphi_{y,c}}{A}\right)^2=1 \tag{49}$$

$$\left(1-y^2\right)\left(sin\,\varphi_{y,c}\right)^2-2A\ sin\,\varphi_{y,c}+\ y^2=0 \tag{50}$$

Coefficients of quadratic equations are

$$a=\left(1-y^2\right),\ b=-2A \text{ and } c=y^2.$$

From the value of $sin(\phi_{y,c})$ by quadratic solution, $\phi_{y,c}$ can be determined.

Collectively, these expressions indicate, The harmonic voltage phase angle shifts both the timing and value of the supply voltage peak, as shown in equations (15)-(23) and Figures 12–14. These peak changes follow a periodic pattern with harmonic phase variation.

VI. RESULTS AND VERIFICATION

From (44) and (50)

$$\varphi_{peak} = cos^{-1}\left\{\frac{-(-2)\pm\sqrt{(-2)^2-4\left(1-\frac{1}{y^2}\right)\left(1+\frac{1}{y^2}-\frac{1}{A^2}\right)}}{2\left(1-\frac{1}{y^2}\right)}\right\} \tag{51}$$

$$\varphi_{y,c} = sin^{-1}\left\{\frac{-(-2A)\pm\sqrt{(-2A)^2-4\left(1-y^2\right)y^2}}{2\left(1-y^2\right)}\right\} \tag{52}$$

Mathematically, every quadratic equation has two possible solutions. Depending on the coefficient values, one or both of these solutions may yield a complex result. Equation (24) determines the distance between the zero crossing of the harmonic component and the modified peak of the resultant waveform. Out of the two solutions, only the positive-real solution is used as the argument for the inverse sine function ($\sin^{-1}$) in equation (24). For U_{yRMS} =10V and U_{1RMS} = 230V, the value of A is 23, and $y = 5$ for the 5th harmonic. The quadratic solutions in this case are 0.442 and –2.36. Since the argument for the inverse sine function must be within the range [−1,1][-1, 1][−1,1], only one solution is valid:

$$\varphi_{y,c}=\sin^{-1}(0.442)=\begin{cases}26.3^\circ\\ -26.3^\circ\end{cases}$$

It should be noted that $\phi_{y,c}$ is scaled by y on the fundamental harmonic scale, which corresponds to 5.3°. Furthermore, $\phi_{y,c}$ represents the exact instant where the $u_1(t)$ and $u_{LVAC}(t)$ waveforms intersect (see FIGURE 16). Similarly, ϕ_{peak} can be calculated using the inverse cosine ($\cos^{-1}$) function applied to the quadratic solution in (44). For the given harmonic amplitudes and voltage harmonic order, the $\cos^{-1}$ argument values are 1.103 and 0.981. Like the sine function, the cosine argument must also lie within the range [−1,1][-1, 1][−1,1]. Therefore:

$$\varphi_{peak}=\cos^{-1}(0.981)=78.8^\circ$$

Hereby, the peak shift for the fundamental component timing will be

$$\varphi\Delta_{peak}=\left|90^\circ-78.8^\circ\right|=11.2^\circ$$

The results align closely with empirical values, as shown in FIGURE 17 and Tables 2 and 3, confirming the accuracy of the developed equations. The calculated values for ϕ_{Upeak}, $\Delta\phi_{peak}$, and $\phi_{\text{y,c}}$ exhibit strong consistency with the measured values presented in FIGURE 17 and Table 3. The shift in peak phase instant, $\Delta\phi_{Upeak}$, can be expressed in terms of an equivalent time, $t_{peak,\Delta U=0}$. FIGURE 17 illustrates the measured phase angle values corresponding to these calculations.

Table 3 provides the calculated values for the maximum shift in peak phase instant ($\Delta\varphi_{peak,max}$) and the maximum shift in peak time instant ($t_{peak,\Delta\phi,max}$) under Case 1, as derived from equation (30). Notably, an increase in the amplitude of higher-order harmonics (e.g., the 7th harmonic) can result in multiple or equal peak values in the voltage waveform. In such instances, the calculation identifies only the dominant peak value among the possible alternatives.

Further, Table 3 compares measured and calculated values for the peak phase instant and the zero-crossing instants of the harmonic component, based on equations (50) and (51) under Case 2. The high level of agreement between these values validates the precision of the developed equations. This accuracy is further reinforced through comparisons with recorded measurements for specific harmonic amplitudes and phase angles, as demonstrated in Table 4.

Figure 17 presents the ΔU_{peak} and $\Delta\varphi_{peak}$ values for u_{LVAC}(t) incorporating the 3rd harmonic voltage. The figure illustrates variations in the 3rd harmonic voltage phase angle (φ_{U3}) over a full cycle (0° to 360°), encompassing all discussed cases. Additionally, Table 2 compares experimental and analytical results across different harmonic conditions, revealing minor deviations in peak voltage timing and magnitude. While these discrepancies highlight the limitations of the current analytical framework under higher-order harmonic influences, the quantitative comparison underscores the robustness of the proposed model across a range of practical scenarios.

The determination of these characteristic points is essential, as they define the maximum, minimum, and zero-crossing points of the periodic variation in $\Delta\phi_{peak}$ and peak magnitude. However, as observed in FIGURE 17, these periodic variations do not exhibit a purely sinusoidal nature, as suggested by Equations (22) and (23), but rather resemble the behavior described by Kepler's equation.

An approximate (series) solution can be employed to accurately calculate or model the peak instant time and peak magnitude when a voltage harmonic is introduced at a

TABLE 2. Modeled/calculated value of maximum peak stretch on the time axis for any level of influencer harmonic.

Harmonic Order y	U_{yRMS}, V	$\varphi_{peak,max}$, °	$t_{peak,\Delta\varphi max}$, ms
3rd	5	86.3	4.79
	10	82.5	4.58
	15	78.7	4.37
	20	74.9	4.16
	25	71.0	3.94
5th	5	83.8	4.65
	10	77.4	4.30
	15	71.0	3.94
	20	64.2	3.57
	25	57.1	3.17
7th	5	81.2	4.51
	10	72.3	4.02
	15	62.8	3.49

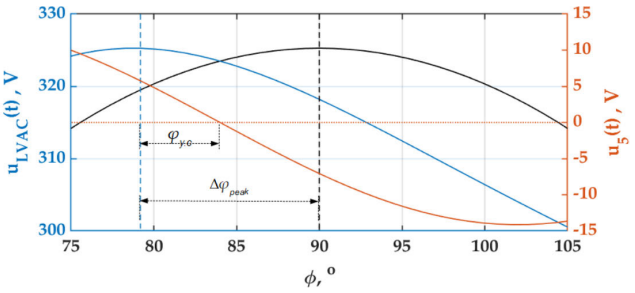

FIGURE 16. Distance calculation of zero crossing for influencer harmonic and fundamental components peak toward peak instant of $u_{LVAC}(t)$.

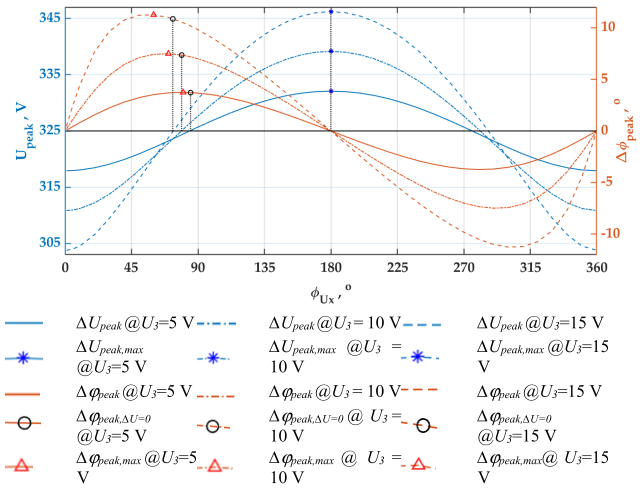

FIGURE 17. Results of U_{peak} and φ_{Upeak} instant of $u_{LVAC}(t)$.

specific phase angle, expressed by the expression below:

$$\varphi_{peak,ss} = \frac{\pi}{2} + (-1)^{\frac{y+1}{2}}\left(\left(\frac{U_y}{U_1}y\right) - \frac{1}{8}\left(\frac{U_y}{U_1}\right)^3 y^3(3y-1) \times(3y+1))\, sin\left(\varphi_y\right) + \frac{y^3}{2}\left(\frac{U_y}{U_1}\right)^2 sin\left(2\varphi_y\right) \quad (53)$$

TABLE 3. Comparison of measured and calculated value of resultant peak stretch of $u_{LVAC}(t)$, magnitude identical to the fundamental component.

y	U_{yRMS}, V	$\varphi_{peak,meas}$, °	$\varphi_{peak,calc}$ °	$\varphi_{y,c,meas}$ °	$\varphi_{y,c,calc}$ °	$\varphi_{cross,y,meas}$ °	$\varphi_{cross,y,calc}$ °
3	5	86.3	**86.3**	6.2	**5.6**	87.9	**88.1**
	10	82.6	**82.6**	11.1	**10.9**	86.3	**86.4**
	15	79.1	**79.2**	15.6	**15.9**	84.8	**84.7**
	20	75.9	**75.8**	20.4	**20.4**	83.2	**83.2**
	25	72.8	**72.7**	24.7	**24.5**	81.8	**81.8**
5	5	84.0	**84.0**	14.2	**14.8**	87.2	**87.0**
	10	78.8	**78.8**	26.2	**26.2**	84.8	**84.8**
	15	74.4	**74.4**	34.2	**34.4**	83.2	**83.1**
	20	70.7	**70.7**	40.5	**40.4**	81.9	**81.9**
	25	67.4	**67.4**	45.0	**45.0**	81.0	**81.0**
7	5	82.1	**82.1**	26.1	**25.7**	86.3	**86.3**
	10	76.6	**76.5**	40.6	**39.7**	84.2	**84.3**
	15	72.3	**72.1**	48.1	**47.7**	83.1	**83.2**

TABLE 4. Measured values at characteristic points of resultant peak phase stretch of $u_{LVAC}(t)$.

case	y	3		5	
	U_{yRMS}, V	$\Delta\varphi_{peak}$,°	φ_y, °	$\Delta\varphi_{peak}$,°	φ_y, °
$\Delta\varphi_{peak}$ = max	5	3.8	80	6.2	120
	10	7.5	68	12.6	155
	15	11.3	55	18.8	185
$\Delta U_{peak} = 0$	5	3.7	85	6.0	105
	10	7.4	79	11.3	120
	15	10.9	73	15.7	135
ΔU_{peak} = (max/min)	5	0	0; 180	0	0; 180
	10				
	15				

This approach enables the prediction of the expected peak value and its corresponding time instant for any given phase angle of the influencing voltage harmonic. However, the accuracy of the series solution is more reliable for lower harmonic voltage magnitudes, particularly when the 3rd harmonic voltage is below 10 V.

Table 5 presents the measured peak voltage and the measured phase instant of the maximum value of $u_{LVAC}(t)$ when the phase angle of the added 3rd voltage harmonic is varied over 360 degrees, with a harmonic magnitude of 7 V. The deviations between the measured and calculated phase instants of the peak value are minimal.

Table 6 compares the deviations between calculated (using equation (53)) and measured values for various levels of 3rd and 5th harmonic voltages. The results indicate that as the harmonic magnitude increases, the root mean square error (RMSE) also increases, demonstrating the impact of higher harmonic levels on deviation accuracy

The presence of harmonics in the voltage supply waveform can lead to the formation of localized peaks, as illustrated in FIGURE 18. Various power quality standards define permissible limits for different voltage harmonic orders [50], [51], [52] including IEC 61000-2-2 (voltage harmonic limits for

TABLE 5. Measured and calculated values of resultant peak phase stretch of $u_{LVAC}(t)$, when the magnitude of added third harmonic (U_3, rms) is 7V.

φ_3 , °	U_{peak}, V	$\varphi_{peak,mea}$, °	$\varphi_{peak,ss}$, °	φ_{peak}- $\varphi_{peak,ss}$, °
0	315.1	90	90	0
10	315.3	91.2	91.1	0.2
20	315.9	92.4	92.1	0.3
30	316.9	93.4	93.0	0.4
40	318.1	94.2	93.8	0.4
50	319.6	94.7	94.4	0.3
60	321.2	95.1	94.8	0.3
70	322.9	95.2	95.0	0.3
80	324.6	95.2	95.0	0.3
90	326.3	95.1	94.8	0.3
100	327.9	94.8	94.5	0.3
110	329.5	94.4	94.0	0.3
120	330.8	93.9	93.5	0.4
130	332.0	93.4	93.0	0.4
140	333.0	92.8	92.4	0.4
150	333.8	92.1	91.8	0.3
160	334.4	91.4	91.2	0.2
170	334.8	90.7	90.6	0.1
180	334.9	90.0	90.0	0.0
190	334.8	89.3	89.4	0.1
200	334.4	88.6	88.8	0.2
210	333.8	87.9	88.2	0.3
220	333.0	87.2	87.6	0.4
230	332.0	86.6	87.0	0.4
240	330.8	86.1	86.5	0.4
250	329.5	85.6	86.0	0.3
260	327.9	85.2	85.5	0.3
270	326.3	84.9	85.2	0.3
280	324.6	84.8	85.0	0.3
290	322.9	84.8	85.0	0.3
300	321.2	84.9	85.2	0.3
310	319.6	85.3	85.6	0.3
320	318.1	85.8	86.2	0.4
330	316.9	86.6	87.0	0.4
340	315.9	87.6	87.9	0.3
350	315.3	88.8	88.9	0.2
			RMSE	0.1

TABLE 6. Difference of measured and calculated (series solution) values of resultant peak phase stretch of $u_{LVAC}(t)$ for various levels of added harmonic.

Harmonic y	3			5		
$U_{y,rms}$, V	1	3	5	1	3	5
φ_y , °	$\varphi_{peak,\,mea}$ - $\varphi_{peak,ss}$, °					
0	0	0	0	0	0	0
10	0.00	0.01	0.06	0.01	0.13	0.50
20	0.00	0.02	0.10	0.01	0.24	1.00
30	0.00	0.03	0.13	0.01	0.33	1.40
40	0.00	0.03	0.14	0.01	0.38	1.70
50	0.00	0.03	0.13	0.01	0.40	1.80
60	0.00	0.03	0.11	0.01	0.39	1.80
70	0.00	0.02	0.10	0.01	0.35	1.70
80	0.00	0.02	0.09	0.01	0.31	1.50
90	0.00	0.02	0.10	0.01	0.27	1.36
100	0.00	0.02	0.11	0.01	0.25	1.20
110	0.00	0.03	0.12	0.01	0.26	1.13
120	0.00	0.03	0.14	0.01	0.29	1.17
130	0.00	0.03	0.14	0.01	0.33	1.30
140	0.00	0.03	0.14	0.01	0.36	1.40
150	0.00	0.03	0.12	0.01	0.36	1.60
160	0.00	0.02	0.09	0.01	0.30	1.50
170	0.00	0.01	0.05	0.01	0.17	0.90
180	0.00	0.00	0.00	0.00	0.00	0.00
RMSE	0.00	0.00	0.01	0.00	0.09	1.82

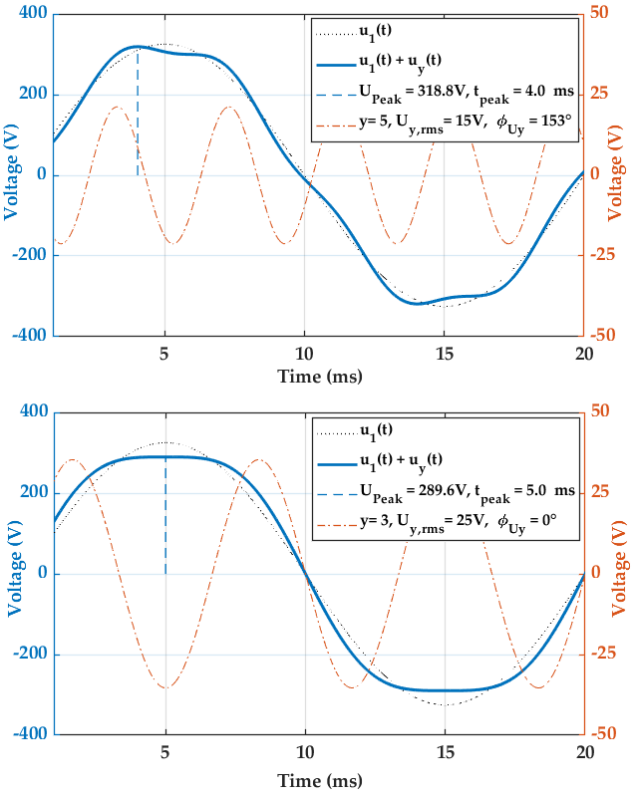

FIGURE 18. Multiple local peak in supply voltage.

low-voltage networks), and IEC 61000-3-2 (harmonic current limits for equipment ≤16 A).

According to IEC 61000-2-2, the permissible limit for dominant odd harmonics typically ranges between 5% and 6% of the fundamental component's magnitude. This limit varies accordingly with a nominal fundamental voltage of 325V peak (230V RMS). The threshold for multiple peaks occurring within a half-cycle can be defined by the relation between the fundamental voltage magnitude and the order of the influencing harmonic, expressed as $U1/y^2$. For instance, the onset of multiple peaks in the supply waveform occurs at 25.5V RMS ($230/3^2$) for the 3rd harmonic, 9V RMS ($230/5^2$) for the 5th harmonic, and 4.68V RMS ($230/7^2$) for the 7th harmonic. At these threshold levels, the resultant waveform exhibits a flattening of peak values over time, particularly for specific phase angles of the harmonic component. This flattening effect is observed for specific values of harmonic phase angle, i.e. for 3rd voltage harmonic, this happened on phase angle 0.

In brief, the Quadratic and trigonometric equations (51)–(53) determine the peak phase and peak time shifts in $u_{LVAC}(t)$ due to voltage harmonics. Measured and calculated values for peak shifts and zero crossings show close agreement, confirming the model's accuracy across harmonic conditions (see Figure 17, Tables 2–6).

VII. CONCLUSION

Analytical expressions for peak voltage levels and timing have been derived for key points in waveform analysis. The solutions to these quadratic expressions reveal that peak voltage and timing phases follow $\sin^{-1}$ or $\cos^{-1}$ functions. Notably, for small arguments, these functions demonstrate a response which may seem linear in empirical assessments. Nevertheless, as the harmonic order increases, even the 7th harmonic voltage component can introduce nonlinear effects, thereby disrupting this seemingly linear behaviour.

These expressions highlight the near-elliptical relationship between rectifier circuit harmonic load components on the complex plane. Nevertheless, these expressions partially characterize the DC-side behavior of the rectifier, regarding the anticipated load current in the presence of distorted supply voltages. The analysis operates under an idealized framework, overlooking certain circuit characteristics that may result in minor deviations in the actual peak voltage of the capacitor and its timing. These findings optimize rectifier-based circuits by improving capacitor sizing and harmonic filtering, ensuring stability under supply distortions while enhancing power electronics design.

Future work will focus first on finding the analytical solution of other characteristic points U_{init} , t_{init} and I_{init} and further extending the analytical framework by incorporating multiple voltage harmonic components. The inclusion of voltage harmonics increases the complexity of the Fourier transform, leading to non-linear functions shaped by geometric interrelations. Although idealized waveforms serve as the basis for analysis, the derived expressions introduce difficult-to-integrate mathematical concepts. The complexity demands efficient reduction techniques, as certain periodic functions, similar to the Kepler function, remain analytically unresolved. Consequently, the approach is constrained to estimating characteristic points rather than obtaining closed-form solutions. Further refinement of the mathematical formulations will be a key aspect of future research.

REFERENCES

[1] A. Mansoor, W. M. Grady, R. S. Thallam, M. T. Doyle, S. D. Krein, and M. J. Samotyj, "Effect of supply voltage harmonics on the input current of single-phase diode bridge rectifier loads," *IEEE Trans. Power Del.*, vol. 10, no. 3, pp. 1416–1422, Jul. 1995, doi: 10.1109/61.400924.

[2] M. Jarkovoi, M. N. Iqbal, and L. Kütt, "Analysis of harmonic current stability and summation of LED lamps," in *Proc. Electr. Power Quality Supply Rel. Conf. (PQ) Symp. Electr. Eng. Mechatronics (SEEM)*, Jun. 2019, pp. 1–8, doi: 10.1109/PQ.2019.8818237.

[3] A. M. Blanco, S. Yanchenko, J. Meyer, and P. Schegner, "Impact of supply voltage distortion on the current harmonic emission of non-linear loads," *DYNA*, vol. 82, no. 192, pp. 150–159, Aug. 2015, doi: 10.15446/dyna.v82n192.48591.

[4] W. M. Grady, A. Mansoor, E. F. Fuchs, P. Verde, and M. Doyle, "Estimating the net harmonic currents produced by selected distributed single-phase loads: Computers, televisions, and incandescent light dimmers," in *Proc. IEEE Power Eng. Soc. Winter Meeting. Conf.*, vol. 2, Jan. 2002, pp. 1090–1094, doi: 10.1109/PESW.2002.985179.

[5] L. Kütt, E. Saarijärvi, M. Lehtonen, H. Molder, and J. Niitsoo, "Estimating the harmonic distortions in a distribution network supplying EV charging load using practical source data-case example," in *Proc. IEEE Power Energy Soc. Gen. Meet.*, Oct. 2014, pp. 4–8, doi: 10.1109/PESGM.2014.6939267.

[6] M. N. Iqbal, L. Kütt, K. Daniel, B. Asad, and P. S. Ghahfarokhi, "Estimation of harmonic emission of electric vehicles and their impact on low voltage residential network," *Sustainability*, vol. 13, no. 15, p. 8551, Jul. 2021, doi: 10.3390/su13158551.

[7] A. Bhowmik, A. Maitra, S. M. Halpin, and J. E. Schatz, "Determination of allowable penetration levels of distributed generation resources based on harmonic limit considerations," *IEEE Trans. Power Del.*, vol. 18, no. 2, pp. 619–624, Apr. 2003, doi: 10.1109/TPWRD.2003.810494.

[8] T. Busatto, S. K. Rönnberg, and M. H. J. Bollen, "Comparison of models of single-phase diode bridge rectifiers for their use in harmonic studies with many devices," *Energies*, vol. 15, no. 1, p. 66, Dec. 2021, doi: 10.3390/en15010066.

[9] S. R. Hassan, A. Rehman, N. Shabbir, and A. Unbreen, "Comparative analysis of power quality monitoring systems," *NFC IEFR J. Eng. Sci. Res.*, vol. 7, no. 1, pp. 19–23, Dec. 2019, doi: 10.24081//nijesr.2019.1.0004.

[10] M. N. Iqbal, L. Kütt, N. Shabbir, and B. Asad, "Comparison of current harmonic emission by different lighting technologies," in *Proc. IEEE 61th Int. Sci. Conf. Power Electr. Eng. Riga Tech. Univ. (RTUCON)*, Nov. 2020, pp. 1–6, doi: 10.1109/RTUCON51174.2020.9316615.

[11] M. Rylander, W. M. Grady, and M. Narendorf, "Experimental apparatus, testing results, and interpretation of the impact of voltage distortion on the current distortion of typical single-phase loads," *IEEE Trans. Power Del.*, vol. 24, no. 2, pp. 844–851, Apr. 2009, doi: 10.1109/TPWRD.2008.2002874.

[12] K. Daniel, L. Kütt, M. N. Iqbal, N. Shabbir, M. Jarkovoi, and M. Parker, "Voltage main harmonic level influence on harmonic current emission modeling," in *Proc. Int. Conf. Future Energy Solutions (FES)*, Jun. 2023, pp. 1–6, doi: 10.1109/fes57669.2023.10183302.

[13] M. M. Silva, M. Losada y Gonzalez, and S. R. Silva, "A new analytical model for evaluating loads supplied by sinusoidal and non-sinusoidal voltage sources," in *Proc. IEEE/PES Transmiss. Distrib. Conf. Expo., Latin Amer. (T&D-LA)*, Nov. 2010, pp. 824–831, doi: 10.1109/TDC-LA.2010.5762980.

[14] W. Ryckaert, J. Ghijselen, and J. Melkebeek, "Harmonic mitigation potential of shunt harmonic impedances and the influence of background distortion," in *Proc. IEEE Bol. PowerTech Conf.*, Jul. 2004, pp. 8–15, doi: 10.1109/PTC.2003.1304626.

[15] M. Montigny and P. Sicard, "Harmonic modeling of a cluster of AC/DC converters," in *Proc. IEEE Int. Symp. Ind. Electron.*, Jul. 2006, pp. 1846–1851, doi: 10.1109/ISIE.2006.295853.

[16] J. J. Mesas, L. Sainz, and J. Molina, "Parameter estimation procedure for models of single-phase uncontrolled rectifiers," *IEEE Trans. Power Del.*, vol. 26, no. 3, pp. 1911–1919, Jul. 2011, doi: 10.1109/TPWRD.2011.2120629.

[17] M. Chen, C. Zheng, Z. Qian, and X. Yuan, "The analysis of inverter under rectifier load using a nonlinear rectifier model," in *Proc. INTELEC 27th Int. Telecommun. Conf.*, Sep. 2005, pp. 455–459, doi: 10.1109/INTLEC.2005.335141.

[18] J. E. Hernandez, R. P. Kandula, F. Lambert, D. Divan, and S. Grijalva, "A 7.2 kV experimental setup of a third harmonic hybrid active filter for medium voltage utility applications," in *Proc. IEEE Energy Convers. Congr. Expo. (ECCE)*, Sep. 2013, pp. 5199–5206, doi: 10.1109/ECCE.2013.6647404.

[19] Z. Chen, Y. Han, Y. Wu, Z. Lu, and X. Liu, "A low voltage stress PFC rectifier based on nonoverlapping strategy using resonant switched-capacitor converter," *IEEE Trans. Ind. Electron.*, vol. 69, no. 12, pp. 12728–12738, Dec. 2022, doi: 10.1109/TIE.2021.3135643.

[20] S. Yanchenko and J. Meyer, "Harmonic emission of household devices in presence of typical voltage distortions," in *Proc. IEEE Eindhoven PowerTech, PowerTech*, Jun. 2015, pp. 1–6, doi: 10.1109/PTC.2015.7232518.

[21] A. M. Blanco, R. Stiegler, and J. Meyer, "Power quality disturbances caused by modern lighting equipment (CFL and LED)," in *Proc. IEEE Grenoble Conf. PowerTech (POWERTECH)*, Jun. 2013, pp. 1–6, doi: 10.1109/PTC.2013.6652431.

[22] M. Rawa, D. W. P. Thomas, and M. Sumner, "Power quality monitoring and simulation of a personal computer based on IEEE 1459–2010," in *Proc. IEEE Int. Symp. Electromagn. Compat.*, Nov. 2013, pp. 671–675.

[23] A. S. Folting, J. Myrzik, T. Wiesner, and L. Jendernalik, "Practical implementation of the coupled Norton approach for nonlinear harmonic models," in *Proc. Power Syst. Comput. Conf. (PSCC)*, vol. 1, Aug. 2014, pp. 1–7, doi: 10.1109/PSCC.2014.7038372.

[24] D. Lv, J. Zhang, and Y. Dai, "Study on time and frequency-domain harmonic models of single-phase full bridge rectifiers," in *Proc. IEEE Int. Conf. Cyber Technol. Autom. Control Intell. Syst. (IEEE-CYBER)*, Jun. 2015, pp. 1186–1191, doi: 10.1109/CYBER.2015.7288112.

[25] K. Daniel, L. Kütt, M. N. Iqbal, N. Shabbir, and M. Jarkovoi, "Description of practical load harmonic current emission due to voltage harmonic variation," in *Proc. IEEE 62nd Int. Sci. Conf. Power Electr. Eng. Riga Tech. Univ. (RTUCON)*, Nov. 2021, pp. 1–6, doi: 10.1109/RTUCON53541.2021.9711594.

[26] C. F. M. Almeida and N. Kagan, "Harmonic coupled Norton equivalent model for modeling harmonic-producing loads," in *Proc. 14th Int. Conf. Harmon. Quality Power (ICHQP)*, Sep. 2010, pp. 1–9, doi: 10.1109/ICHQP.2010.5625491.

[27] F. Yahyaie and P. W. Lehn, "Using frequency coupling matrix techniques for the analysis of harmonic interactions," *IEEE Trans. Power Del.*, vol. 31, no. 1, pp. 112–121, Feb. 2016, doi: 10.1109/TPWRD.2015.2442573.

[28] J. Yadav, K. Vasudevan, J. Meyer, and D. Kumar, "Frequency coupling matrix model of a three-phase variable frequency drive," *IEEE Trans. Ind. Appl.*, vol. 58, no. 3, pp. 3652–3663, May 2022, doi: 10.1109/TIA.2022.3156104.

[29] M. N. Iqbal, L. Kütt, M. Lehtonen, R. J. Millar, V. Püvi, A. Rassõlkin, and G. L. Demidova, "Travel activity based stochastic modelling of load and charging state of electric vehicles," *Sustainability*, vol. 13, no. 3, p. 1550, Feb. 2021, doi: 10.3390/su13031550.

[30] G. Ye, M. Nijhuis, V. Cuk, and J. F. G. Cobben, "Stochastic residential harmonic source modeling for grid impact studies," *Energies*, vol. 10, no. 3, p. 372, Mar. 2017, doi: 10.3390/en10030372.

[31] O. Lennerhag and M. H. J. Bollen, "A stochastic aggregate harmonic load model," *IEEE Trans. Power Del.*, vol. 35, no. 5, pp. 2127–2135, Oct. 2020, doi: 10.1109/TPWRD.2019.2961790.

[32] A. Heidary, H. Radmanesh, and K. Ghorbanyan, "Effect of electronic load in increasing shunt capacitor bank current," in *Proc. 21st Conf. Electr. Power Distrib. Netw. Conf. (EPDC)*, Apr. 2016, pp. 98–101, doi: 10.1109/EPDC.2016.7514790.

[33] S. Maulik and V. John, "Diode bridge rectifier with low THD for weak grids," in *Proc. IEEE Transp. Electrific. Conf. (ITEC-India)*, Dec. 2019, pp. 1–6, doi: 10.1109/ITEC-India48457.2019.ITECINDIA2019-224.

[34] G. Malagon-Carvajal, C. Duarte, G. Ordonez-Plata, C. F. M. Almeida, and N. Kagan, "Harmonic attenuation-amplification effect on lighting branch circuits," in *Proc. IEEE 6th Int. Conf. Renew. Energy Res. Appl. (ICRERA)*, Nov. 2017, pp. 283–289, doi: 10.1109/ICRERA.2017.8191280.

[35] C. L. Collocott, K. O. Awodele, and A. V. Adebayo, "Harmonic emission of non-linear loads in distribution Systems–A computer laboratory case study," in *Proc. Int. SAUPEC/RobMech/PRASA Conf.*, Jan. 2020, pp. 1–6, doi: 10.1109/SAUPEC/RobMech/PRASA48453.2020.9041104.

[36] S. Yanchenko, "Harmonic phenomena of typical low-distortion residential equipment," in *Proc. 2nd Int. Conf. Ind. Eng., Appl. Manuf. (ICIEAM)*, May 2016, pp. 1–6, doi: 10.1109/ICIEAM.2016.7910992.

[37] S. Gopalan, K. Vasudevan, and D. Kumar, "Impact of inductor placement on DC bus capacitor of adjustable speed drives under non-ideal supply voltage conditions," *Electr. Power Compon. Syst.*, vol. 51, no. 7, pp. 669–683, Apr. 2023, doi: 10.1080/15325008.2023.2180816.

[38] M. H. Rashid, "Power electronics circuits devices and application," Tech. Rep., 2014. [Online]. Available: https://www.amazon.com/Power-Electronics-Circuits-Devices-Applications/dp/0133125904

[39] A. Tokic, A. Jukan, and J. Smajic, "Parameter estimation of single-phase rectifier-based loads: Analytical approach," *IEEE Trans. Power Del.*, vol. 31, no. 2, pp. 532–540, Apr. 2016, doi: 10.1109/TPWRD.2015.2424914.

[40] *Electromagnetic Compatibility (EMC) Part 4-30: Testing and Measurement Techniques Power Quality Measurement Methods*, document IEC 61000-4-30:2003, Int. Electrotech. Commun., 2003.

[41] K. Daniel, L. Kütt, M. N. Iqbal, N. Shabbir, M. Parker, and M. Jarkovoi, "Waveform variation defined model for harmonic current emissions including cross-order supply voltage harmonics influence," *IEEE Access*, vol. 11, pp. 42276–42289, 2023, doi: 10.1109/ACCESS.2023.3270805.

[42] J. Liu, J. K. Motwani, D. Zhang, and D. Dong, "Unidirectional hybrid multilevel rectifier family for MV/HV applications: Analysis and comparative evaluation," *IEEE Trans. Power Electron.*, vol. 39, no. 3, pp. 3300–3312, Mar. 2024, doi: 10.1109/TPEL.2023.3337772.

[43] S. Gupta, N. Vamanan, and V. John, "A diode bridge rectifier with improved power quality using the capacitive network," *IEEE Trans. Ind. Appl.*, vol. 54, no. 2, pp. 1563–1572, Mar. 2018, doi: 10.1109/TIA.2017.2785354.

[44] X. Yue and S. Du, "A synchronized switch harvesting rectifier with reusable storage capacitors for piezoelectric energy harvesting," *IEEE J. Solid-State Circuits*, vol. 58, no. 9, pp. 1–10, Sep. 2023, doi: 10.1109/JSSC.2023.3260145.

[45] X. Xie, J. Zhang, Y. Sun, and J. Fan, "A measurement-based dynamic harmonic model for single-phase diode bridge rectifier-type devices," *IEEE Trans. Instrum. Meas.*, vol. 73, pp. 1–13, 2024, doi: 10.1109/TIM.2024.3370782.

[46] J.-K. Han, J.-W. Kim, and G.-W. Moon, "A high-efficiency asymmetrical half-bridge converter with integrated boost converter in secondary rectifier," *IEEE Trans. Power Electron.*, vol. 32, no. 11, pp. 8237–8242, Nov. 2017, doi: 10.1109/TPEL.2017.2675283.

[47] S. Sharifi, M. Monfared, and M. Babaei, "Ferdowsi rectifiers—Single-phase buck-boost bridgeless PFC rectifiers with low semiconductor count," *IEEE Trans. Ind. Electron.*, vol. 67, no. 11, pp. 9206–9214, Nov. 2020, doi: 10.1109/TIE.2019.2955430.

[48] S. Elphick, P. Ciufo, and S. Perera, "Laboratory investigation of the input current characteristics of modern domestic appliances for varying supply voltage conditions," in *Proc. 14th Int. Conf. Harmon. Quality Power (ICHQP)*, Sep. 2010, pp. 1–7, doi: 10.1109/ICHQP.2010.5625397.

[49] K. Daniel, L. Kütt, M. N. Iqbal, N. Shabbir, M. Jarkovoi, and M. Parker, "Load current harmonic model complexity reduction through empirical pattern analysis," in *Proc. IEEE 17th Int. Conf. Compat., Power Electron. Power Eng. (CPE-POWERENG)*, Jun. 2023, pp. 1–6, doi: 10.1109/CPE-POWERENG58103.2023.10227474.

[50] *Electromagnetic Compatibility (EMC)-Environment-Compatibility Levels for Low-Frequency Conducted Disturbances and Signalling in Public Low-Voltage Power Supply Systems*, document IEC 61000-2-2:2002/A1:2017, IEC 61000-2-22002/a12017, 2017, p. 37.

[51] E. P. Olme and K.-Ja, *Elektromagnetiline Ühilduvus. OSA 6-3: Electromagnetic Compatibility (EMC)—Part 6-3: Generic Standards-Emission Standard for Equipment in Residential Environments*, Standard EESTI STANDARD EVS-EN IEC 61000-6-3: 2021, 2021.

[52] N. Shabbir, L. Kütt, M. Jarkovoi, M. N. Iqbal, A. Rassõlkin, and K. Daniel, "An overview of measurement standards for power quality," *Agron. Res.*, vol. 19, no. 1, pp. 944–960, Jan. 2021, doi: 10.15159/ar.21.074.

KAMRAN DANIEL (Member, IEEE) received the B.Sc. degree in electronics engineering from The Islamia University of Bahawalpur, in 2008, the M.S. degree from the University of South Asia, Lahore, Pakistan, and Ph.D. degree from the Department of Electrical Power Engineering and Mechatronics, Tallinn University of Technology, Estonia, in 2024. He is currently a Researcher with Tallinn University of Technology and doing a postdoctoral research with Aalto University, Finland. His research interests include network harmonic modeling, power line diagnostics, power quality, and electromagnetic compatibility.

LAURI KÜTT (Senior Member, IEEE) received the B.Sc. degree in computer and automation technology and the M.Sc. degree in electrical power engineering from Tallinn University of Technology, Tallinn, Estonia, in 2002 and 2004, respectively, and the Ph.D. degree from the Department of Energy and Geotechnology, Tallinn University of Technology, in 2012. He is currently a Professor with the Department of Electrical Power Engineering and Mechatronics, Tallinn University of Technology. His current research interests include fast transients on electric power lines, power line diagnostics, power quality, and electromagnetic compatibility.

NOMAN SHABBIR (Senior Member, IEEE) received the B.S. degree in computer engineering from COMSATS, Lahore, Pakistan, the M.S. degree in electrical engineering from BTH, Sweden, and the Ph.D. degree from the Department of Electrical Power Engineering and Mechatronics, Tallinn University of Technology, Estonia, in 2022. He is currently a Research Fellow with the FinEST Center for Smart Cities, Tallinn University of Technology. He is also an Assistant Professor with GC University Lahore, Pakistan. His research interests include renewable energy systems, smart grids, machine learning, and ICT.

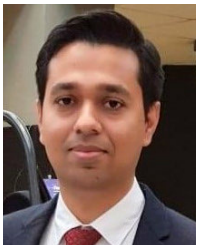

MUHAMMAD NAVEED IQBAL received the B.Sc. degree in electronics engineering from The Islamia University of Bahawalpur, Pakistan, in 2008, the M.S. degree from the University of New South Wales, Australia, in 2010, and the Ph.D. degree from the Department of Electrical Power Engineering and Mechatronics, Tallinn University of Technology, Estonia, in 2021. He is currently a Senior Lecturer at Staffordshire Centre for Renewable and Sustainable Engineering, University of Staffordshire, U.K. His current research interests include power line diagnostics, power quality, and electromagnetic compatibility.

JOÃO F. MARTINS (Senior Member, IEEE) received the degree in electrical engineering from the Instituto Superior Técnico (IST), Technical University of Lisbon, Lisbon, Portugal, in 1990, and the M.Sc. and Ph.D. degrees in electrical engineering from IST, Technical University of Lisbon, in 1996 and 2003, respectively. He is currently with the FCT NOVA, Universidade NOVA de Lisboa, Lisbon, where he is also an Associate Professor with Habilitation, being the Head of the Electrotechnical Engineering and Computers Department. He is also with the Center of Technology and Systems (CTS), UNINOVA, Lisbon, where he coordinates the energy efficiency group and acts as a Communication Officer on the Board of Directors. He has published more than 85 scientific articles in refereed journals and books and more than 180 articles in refereed conference proceedings. His research interests include energy efficiency, alternative energies, and power quality, intelligent and energy-efficient buildings, energy awareness, and smart grid renewables' integration

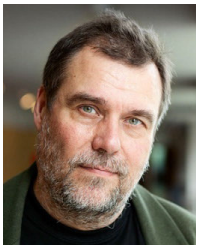

MATTI LEHTONEN (Member, IEEE) received the master's and Licentiate degrees in electrical engineering from Helsinki University of Technology, Finland, in 1984 and 1989, respectively, and the Doctor of Technology degree from Tampere University of Technology, Finland, in 1992. He was with VTT Energy, Espoo, Finland, from 1987 to 2003, and since 1999, has been a Professor at the Aalto University, Espoo, where he is currently the Head of power systems and high voltage engineering. His main activities include power system planning and asset management, power system protection, including earth fault problems, harmonic-related issues, and applications of information technology in distribution systems

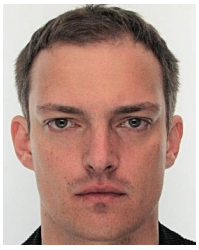

PÄIVO SIMSON received the B.Sc. and M.Sc. degrees in technical physics from Tallinn University of Technology (TalTech), Estonia, in 2006 and 2011, respectively, where he is currently pursuing the Ph.D. degree in technical physics. His research focuses on water waves and nonlinear evolution equations, with an emphasis on analytical and numerical approaches in fluid dynamics. He has also explored magnetostatic problems using conformal mapping. In addition to his research, he is actively involved in physics, mathematics, and engineering education, contributing to national and international competitions by designing and evaluating problems across various fields. His research interests include wave dynamics, nonlinear systems, electromagnetism, and applied mathematical methods in physics.